引用格式：ZHANG Jing, WANG Chong, WANG Yang, et al. Low-stress Near-infrared dichroic Beam-splitting Coatings on Erbium Glass Substrates for Laser Ranging Systems[J]. Acta Photonica Sinica, 2026, 55(1):0131004
张静,王冲,汪洋,等.激光测距系统用铒玻璃基底低应力近红外分光膜[J].光子学报,2026,55(1):0131004

激光测距系统用铒玻璃基底低应力近红外分光膜

张静[1],王冲[1,2],汪洋[3],金海俊[3],曾彬[4],潘永刚[1,2],杨飞[5],黄亚洲[1,2]
(1 长春理工大学 光电工程学院,长春 130022)
(2 长春理工大学中山研究院,中山 528436)
(3 光驰科技(上海)有限公司,上海 200444)
(4 成都晗森光电材料有限公司,成都 611934)
(5 中国科学院长春光学精密机械与物理研究所,长春 130033)

摘 要:基于铒玻璃基底,采用Ta_2O_5和SiO_2作为镀膜材料,并结合中频磁控溅射沉积技术研制了低应力红外分光膜。基于鲁棒性原理,结合镀膜设备沉积工艺,进行膜系设计,引入膜厚误差分析,提高了膜系设计的可制造性;采用控制变量法,建立Ta_2O_5和SiO_2薄膜应力与沉积工艺之间的映射关系,降低了膜层应力,提高了膜层附着力。测试结果表明,在0°角入射下,800~1 000 nm波段的平均反射率为0.16%,1 500~1 600 nm波段的平均反射率为99.87%,膜层残余应力为-105 MPa,并通过附着力试验、高低温循环试验、水煮试验等测试,满足激光测距系统中分光膜使用要求。

关键词:铒玻璃;近红外分光膜;中频磁控溅射;工艺优化;低应力
中图分类号:O484 **文献标识码**:A **doi**:10.3788/gzxb20265501.0131004

0 引言

铒玻璃激光器具有体积小、效率高、光束质量好以及生产成本低等优势,同时1 535 nm是大气窗口波段,穿透力较强,且位于人眼安全范围,能显著降低使用风险[1],被广泛应用于激光测距系统中[2-3],此外在激光雷达以及军事医疗等领域[4-5]也有重要的应用价值。由于铒玻璃具有弱稳定性、亲水性、热膨胀系数大等特性[6-7],导致铒玻璃薄膜器件因应力过大出现膜层附着力变差的问题,已经成为限制铒玻璃激光器发展的技术瓶颈,如何降低铒玻璃薄膜器件的应力,提高膜层附着性已成为国内外学者的研究热点。

近年来,国内外对降低膜层残余应力及提高膜层附着力进行了系列的研究。2017年,袁文佳等[8]通过改变离子源电压研究了Ta_2O_5和SiO_2薄膜的应力变化,随离子源电压的增加,Ta_2O_5和SiO_2薄膜应力呈现先增加后减小的趋势,其薄膜应力变化范围分别为-373~-299 MPa、-577~-427 MPa。2019年,刘保剑等[9]通过提高退火温度可有效降低Ta_2O_5/SiO_2多层高反膜的残余应力,薄膜最低应力为-4.3 MPa。2020年,ELO R等[10]通过增加氮气流量的方式降低了CrN薄膜应力,薄膜应力从340 MPa降低至80 MPa。2021年,朱京涛等[11]通过在不同氩气工作压强下优化Zr薄膜的应力,在大于0.1 Pa工作压强下,Zr薄膜应力随着工作压强减小而缓慢减小。同年,BARTSCHI M等[12]通过增大氩氧化物等离子体源(PSC)功率的方式,有效降低了Ta_2O_5薄膜的应力。2023年,ZHOU Y等[13]通过对玻璃进行化学蚀刻产生连续的凹坑,将SiO_2、SiOC薄膜作为打底层嵌入凹坑中,可有效增加DLC薄膜与玻璃的附着强度。2024年,王通等[14]从膜基材料的热膨胀系数差异入手,通过优化烘烤温度和离子参数来降低薄膜的残余应力,薄膜最低应力为-30 MPa,从而提高了硫系玻璃基底上薄膜的附着力。

基金项目:中山市引进创新团队项目(CXTD2023008),吉林省科技发展计划项目资助(20230101008JC),中国科学院青年创新促进会优秀会员(Y202053),国家自然科学基金(11973040)
第一作者:张静,Zhangjing840225@163.com
通讯作者:王冲,Wangcchong0612@163.com
收稿日期:2025-08-18;**录用日期**:2025-10-16

综上所述，关于降低膜层残余应力、提高薄膜附着力的研究已有诸多报道，然而在铒玻璃基底上实现800～1 000 nm和1 500～1 600 nm双波段分光且保持低应力薄膜的研究鲜有报道。本文采用中频磁控溅射制备了近红外低应力分光膜，采用控制变量法优化氩气(Argon，Ar)流量、靶材(Target，TG)功率、电感耦合等离子体(Inductively Coupled Plasma，ICP)功率三种关键工艺参数，降低Ta_2O_5和SiO_2薄膜应力，提高铒玻璃薄膜器件的附着力。

1 材料的选取与膜系设计

根据激光测距系统技术要求，近红外分光膜的具体技术参数如表1所示。

表1 分光膜技术参数

Table 1 Technical parameters of the beamsplitter coating

Parameter	Specification
Substrate	Erbium glass
Incident angle	0°
Reflectance	＜0.25%@800～1 000 nm
Reflectance	＞99.8%@1 500～1 600 nm

1.1 铒玻璃基底的特性

铒玻璃是一种Er^{3+}、Yb^{3+}共掺杂磷酸盐玻璃，在20 ℃～100 ℃范围内，热膨胀系数为$8.7\times10^{-6}\ K^{-1}$。为准确获得铒玻璃(21 mm×21 mm×2 mm)的光学特性，采用Cary7000分光光度计在0°角入射下对铒玻璃基底进行测量，获得基底透过率与反射率光谱曲线，如图1(a)所示。同时利用Macleod软件中柯西色散模型反演拟合，获得铒玻璃的光学常数，如图1(b)所示，在975 nm处基底折射率为1.541，消光系数为3.7×10^{-4}，在1 535 nm处基底折射率为1.533，消光系数为2×10^{-5}。

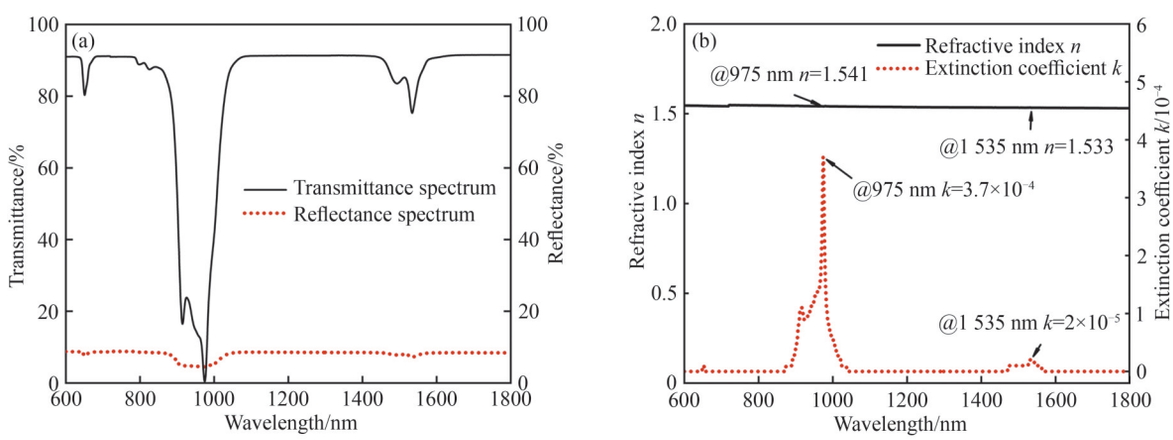


图1 铒玻璃的光学性质。(a)光谱性质；(b) 光学常数

Fig. 1 Optical properties of erbium glass. (a) Spectrum; (b) Optical constants

1.2 薄膜材料的选取

在近红外波段，常用的薄膜材料如表2所示[15]。所查资料[16]可知，SiO_2具有较小的热膨胀系数和低缺陷密度，可有效降低膜层应力，且该材料兼具优良的耐热性，故选用SiO_2作为低折射率材料。常用的高折射率材料有Ti_3O_5、Ta_2O_5、HfO_2，其中钛靶与O_2接触，易发生中毒现象(钛靶材表面与O_2反应形成致密的氧化物层，附着在靶材表面，导致溅射速率骤降)。HfO_2材料应力过大，易引发界面分层[17]，同时在近红外波段Ta_2O_5相对于HfO_2的折射率更大与SiO_2材料匹配需要更少的膜层，故选用Ta_2O_5作为高折射率材料。

表2　常用镀膜材料性质

Table 2　Properties of commonly used coating materials

Materials	Transparent zone/μm	Refractive index(@1 535 nm)	Coefficient of thermal expansion/($\times10^{-6}$ K^{-1})
Ti_3O_5	0.40～14.0	2.26	7.0～9.0 at (25 ℃～300 ℃)
Ta_2O_5	0.30～10.0	2.09	2.5～4.0 at (25 ℃～500 ℃)
HfO_2	0.25～10.0	1.92	5.0～6.5 at (25 ℃～500 ℃)
SiO_2	0.18～8.0	1.45	0.5～0.6 at (2 5℃～1 000 ℃)

1.3　膜系设计

针对红外分光膜(见表1所示)的技术要求，基于光学薄膜设计理论，初始膜系结构选择Sub|(0.5LH0.5L)^5|Air，其中Sub代表铒玻璃，Air代表空气，H代表Ta_2O_5，L代表SiO_2。

正入射时，膜系的反射带宽度计算公式为

$$\Delta g=\frac{2}{\pi}\arcsin\left(\frac{n_H-n_L}{n_H+n_L}\right) \tag{1}$$

$$\Delta\lambda=\frac{\lambda_0}{1-\Delta g}-\frac{\lambda_0}{1+\Delta g}\approx 2\Delta g\cdot\lambda_0 \tag{2}$$

式中，Δg为光子带隙宽度、λ_0为中心波长。将表2中Ta_2O_5和SiO_2材料折射率数据代入式(1)和(2)计算出中心波长1 535 nm处反射带宽为355.2 nm，满足技术指标要求的100 nm反射带宽。

反射率计算公式为

$$R=\frac{n_g-(n_H/n_L)^{2S}n_H^2}{n_g+(n_H/n_L)^{2S}n_H^2} \tag{3}$$

由式(3)可知，当高低折射率比值一定时，反射率随着膜系周期数S增加而增大。当反射率达到99.9%时，通过式(3)计算，膜系周期数S至少为12。因此确定膜系结构为Sub|(0.5LH0.5L)^{12}|Air，利用Macleod软件对膜系设计进行全局优化，优化结果为Sub| 1.06H 0.76L 0.97H 0.86L 1.16H 1.11L 0.93H 0.92L H 1.08L H 0.93L 0.96H 1.06L 1.03H 0.94L 0.93H 1.02L 1.08H 1.02L 0.87H 0.96L 0.75H 0.49L|Air，各膜层物理厚度分布如图2所示，设计光谱曲线如图3所示，800～1 000 nm波段平均反射率为0.076%，1 500～1 600 nm波段平均反射率为99.92%。

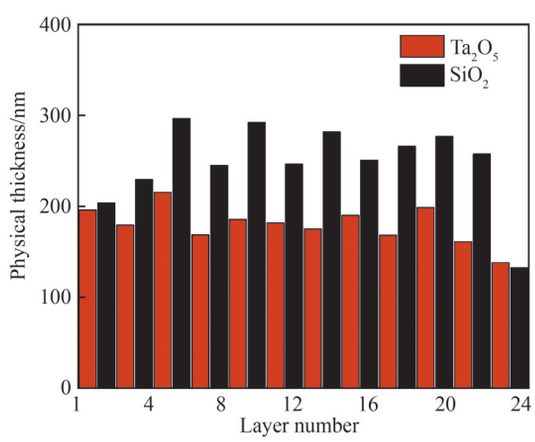


图2　膜系结构示意图

Fig.2　Schematic diagram of the membrane structure

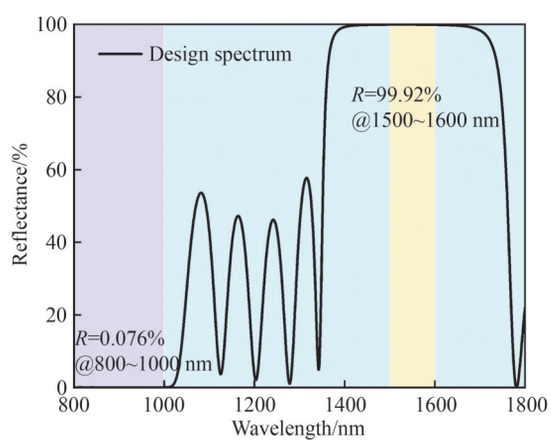


图3　理论设计光谱示意图

Fig.3　Design spectral diagram

为避免敏感层增加薄膜制备的难度，利用Macleod软件中Errors功能对分光膜膜层敏感度进行分析，分析结果如图4所示，第1、3、22层较为敏感。由于沉积的设备膜厚控制使用时间监控，膜厚控制精度约为±1%，因此，对敏感层引入±2%的厚度随机误差，光谱变化如图5所示，可以看出过渡带发生±2 nm的偏移，但分光膜的光谱特性未受影响，满足技术要求。

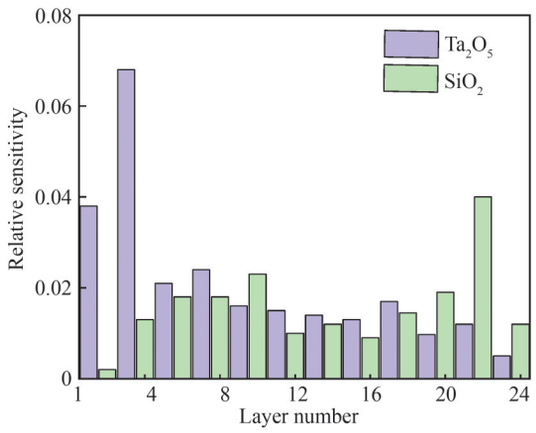


图 4 膜层敏感层分布

Fig.4 Distribution of sensitive layers of membrane layers

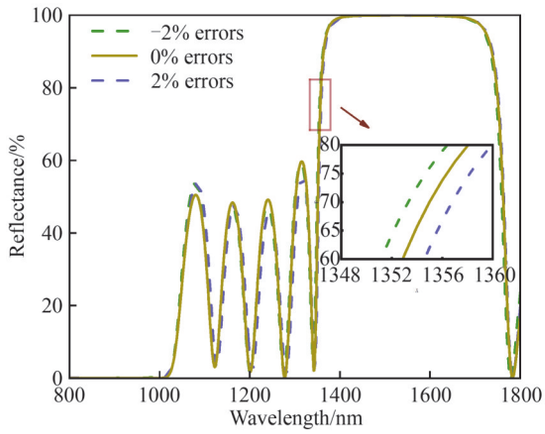


图 5 膜厚误差光谱分析图

Fig.5 Spectral analysis diagram of film thickness error

2 薄膜制备

采用光驰科技(上海)有限公司制造的F1408立式1650型溅射设备,该设备配置2个机械泵-罗茨泵、4台分子泵、2个电感耦合等离子体以及2对喷涂硅靶(TG1、TG2)、1对喷涂钽靶(TG3),腔室布局结构如图6所示。

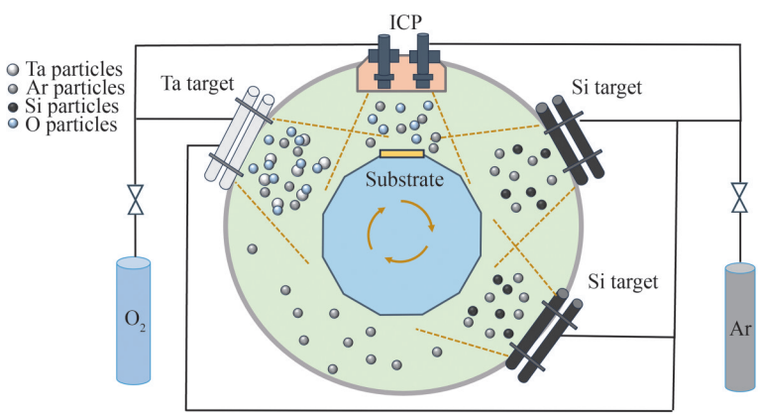


图 6 磁控溅射沉积腔室示意图

Fig.6 Schematic diagram of magnetron sputtering deposition device

在制备前,利用超声波设备对铒玻璃基底进行清洁处理,有效避免灰尘、油脂等杂质导致的脱膜。当真空度达到5.0×10^{-4} Pa时,开启ICP对铒玻璃基底表面进行等离子体轰击,以提升表面活性并提高薄膜的牢固度,具体沉积工艺参数如表3所示。

表 3 沉积工艺参数

Table 3 Deposition process parameters

Material	TG1/TG2-Si		TG3-Ta		ICP×2			Drum rotation/(r·min^{-1})
	Power/kW	Ar/sccm	Ar/sccm	O_2/sccm	Power/kW	Ar/sccm	O_2/sccm	
SiO_2	8	110	110	0	3	100	200	60
Ta_2O_5	7	150	150	0	3	150	300	60

3 测试与分析

3.1 附着力测试与分析

薄膜沉积完成后,对样品进行附着力测试,使用3M胶带粘贴在薄膜表面,垂直快速撕拉5次后,出现脱膜现象,如图7所示。



图7　样品脱膜图
Fig.7　Sample delamination micrograph

综合分析，薄膜脱落主要是由薄膜应力引起，薄膜应力主要由本征应力与热应力构成[18]，针对膜层脱落的问题，主要从工艺参数和镀膜过程中的温度变化进行分析，通过优化沉积工艺参数，降低膜层应力，提高膜层附着力。

基于Stoney公式[19]，结合ET-4000A台阶仪测量并计算薄膜的残余应力，计算公式为

$$\sigma=\frac{E_s}{6(1-\gamma_s)}\frac{t_s^2}{t_f}\left(\frac{1}{R_1}-\frac{1}{R_2}\right) \tag{4}$$

式中，铒玻璃的杨氏模量E_s=72 GPa；泊松比γ_s=0.22；厚度t_s=2 mm；t_f为膜层厚度（单层Ta_2O_5和SiO_2薄膜厚度分别为400 nm和1 000 nm），R_1、R_2为镀膜前后曲率半径大小。

热应力的计算公式为

$$\sigma_{thermal}=\frac{E_f}{1-\nu_f}\cdot(\alpha_s-\alpha_f)\cdot\Delta T \tag{5}$$

式中，$\sigma_{thermal}$为热应力、E_f为材料的杨氏模量、ν_f为材料的泊松比、α_s和α_f为基底和材料的热膨胀系数，ΔT为温度变化量。

为了研究沉积工艺对单层膜应力的影响趋势，并获得低应力膜层制备工艺。本文利用控制变量法，优化单层膜的沉积工艺，包括：氩气流量、靶材功率和电感耦合等离子体功率。

1）Ar流量优化

在表3其他工艺参数不变的前提下，只改变Ar流量，研究5种不同Ar流量下制备单层Ta_2O_5和SiO_2薄膜，实验结果如表4所示，采用式（4）计算不同Ar流量下单层膜的应力，如图8所示。

表4　不同Ar流量下Ta_2O_5和SiO_2的真空度和曲率半径

Table 4　Vacuum level and radius of curvature of Ta_2O_5 and SiO_2 films under different argon flow rates

Flow of Ar /sccm	Vacuum/Pa		R_1/m		R_2/m	
	Ta_2O_5	SiO_2	Ta_2O_5	SiO_2	Ta_2O_5	SiO_2
60	3.35×10^{-2}	3.43×10^{-2}	216.7	10 204.1	191.6	185.1
110	4.05×10^{-2}	4.12×10^{-2}	221.7	−4 464.3	199.0	245.0
160	4.37×10^{-2}	4.45×10^{-2}	224.7	1 204.8	204.9	235.2
210	4.73×10^{-2}	4.81×10^{-2}	237.2	−3 816.8	220.3	347.2
260	5.04×10^{-2}	5.12×10^{-2}	228.6	1 557.6	211.7	261.4

由图8可知，Ta_2O_5和SiO_2单层膜应力随Ar流量增加而减小。当Ar流量从60 sccm增至210 sccm时，随着溅射气压的升高，溅射粒子的动能逐渐降低，导致Ta_2O_5和SiO_2薄膜形成疏松多孔的结构特征，薄膜应力显著下降，降幅分别达到46.2%、40.7%。当Ar流量继续增加至260 sccm时，应力改变量小于5 MPa，由于当Ar流量超过210 sccm的临界值后，溅射出来的靶材原子与O_2充分反应形成稳定化合物，形成后的薄膜结

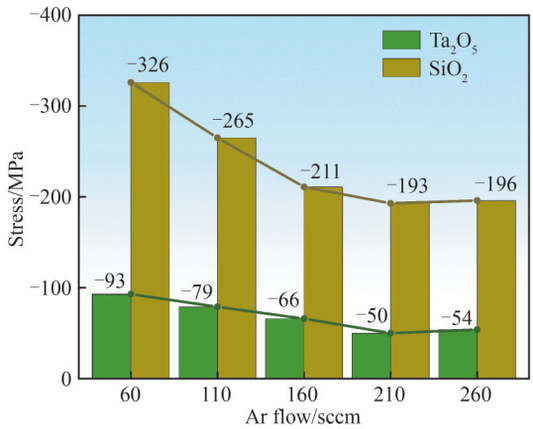


图 8 不同 Ar 流量下 Ta_2O_5 和 SiO_2 的应力演变

Fig. 8 Stress evolution of Ta_2O_5 and SiO_2 films under varying argon flow rates

构已处于饱和状态，薄膜应力变化趋于平缓。过量的 Ar 流量（>210 sccm）不会降低应力调控效果，还会因粗糙度过大导致薄膜发生散射，故 Ta_2O_5 和 SiO_2 薄膜沉积的最佳 Ar 流量设定为 210 sccm。

2）TG 功率优化

采用表 3 中基础工艺参数，分别在 4 种梯度 TG 功率条件下，制备单层 Ta_2O_5 和 SiO_2 薄膜，实验结果如表 5 所示。同时计算不同 TG 功率下单层膜的应力，如图 9 所示。

表 5 不同 TG 功率下 Ta_2O_5 和 SiO_2 薄膜的沉积速率和曲率半径

Table 5 Deposition rate and radius of curvature of Ta_2O_5 and SiO_2 films at different TG power

TG power /kW	Deposition rate/nm·s^{-1}		R_1/m		R_2/m	
	Ta_2O_5	SiO_2	Ta_2O_5	SiO_2	Ta_2O_5	SiO_2
4	0.151	0.633	218.4	−1 577.3	198.1	340.1
6	0.174	0.655	237.3	−1 612.9	215.5	360.2
8	0.204	0.698	144.6	−925.9	133.2	324.3
10	0.216	0.711	114.7	2 415.5	106.5	202.9

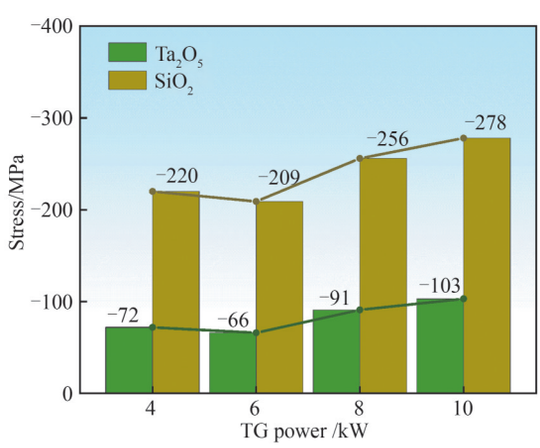


图 9 不同 TG 功率下 Ta_2O_5 和 SiO_2 的应力演变

Fig. 9 Stress evolution of Ta_2O_5 and SiO_2 films under varying TG target power

由图 9 可知，Ta_2O_5 和 SiO_2 单层膜应力随 TG 功率增加呈现出先减小后逐渐增大的趋势。TG 功率可以实现对薄膜沉积速率的调控，当 TG 功率从 4 kW 增至 6 W 时，Ta_2O_5 和 SiO_2 薄膜应力分别降至最低值为 −209 MPa、−66 MPa，两种薄膜材料因厚度和分子结构的差异，其应力变化大小存在不同。而当 TG 功率的继续增至 10 kW 时，沉积速率过快会导致原子迁移受限，缺陷浓度升高，从而引发应力增大[20]，增幅分别达到 56%、33%。为保证薄膜呈现低应力效果，TG 功率确定为 6 kW。

3）ICP功率优化

采用表3中基础工艺参数，分别在4种不同ICP功率条件下制备单层Ta_2O_5和SiO_2薄膜，实验结果如表6所示，并计算不同ICP功率下单层膜的应力，如图10所示。

表6　在不同ICP功率下Ta_2O_5和SiO_2薄膜的温度和曲率半径

Table 6　Temperature and radius of curvature of Ta_2O_5 and SiO_2 films under different ICP powers

ICP power/kW	Temperature/℃		R_1/m		R_2/m	
	Ta_2O_5	SiO_2	Ta_2O_5	SiO_2	Ta_2O_5	SiO_2
0	36	33	246.2	/	223.0	/
1	58	55	234.5	−723.6	209.4	490.2
2	81	85	232.6	−1 483.7	205.8	301.2
3	103	116	160.9	−4 587.2	146.5	244.5

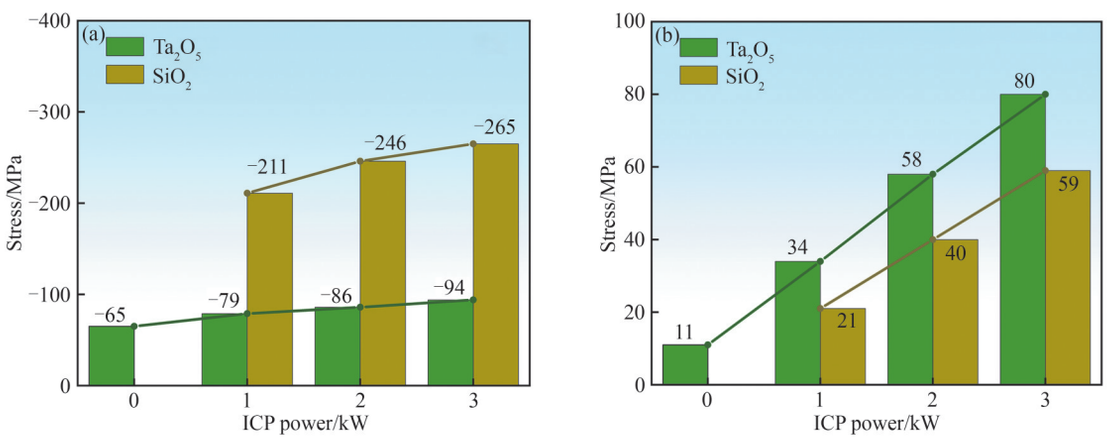


图10　不同ICP功率下Ta_2O_5和SiO_2的残余应力与热应力的变化。(a) 残余应力；(b)热应力

Fig 10　Variation of residual stress and thermal stress in Ta_2O_5 and SiO_2 films under different ICP powers. (a) Residual stress; (b) Thermal stress

如图10(a)所示，Ta_2O_5和SiO_2单层膜残余应力随ICP功率增加而增大。当ICP功率从0增至3kW时，薄膜致密性逐步提高[21]，导致残余应力显著增加，Ta_2O_5和SiO_2薄膜的残余应力分别增加了44.6%和25.6%。随着ICP功率增大，会导致薄膜沉积过程中温度升高，温升数据如表6所示，采用公式(5)计算热应力，如图10(b)所示，与ICP功率呈线性增长关系，表明需要采用低温制备工艺以降低热应力的影响。因此，不采用ICP工艺，有利于膜层应力的减小，然而在充入Ar和O_2流量一定比例的条件下，当SiO_2薄膜无ICP辅助时，O_2离化率较低，形成的化合物为SiO_x($x<2$)，其光学性能和电性能相比较SiO_2会有明显的下降[22]。综合分析，Ta_2O_5薄膜不采用ICP辅助工艺，SiO_2薄膜采用1kW功率的ICP辅助工艺。基于以上分析，经优化后的薄膜沉积工艺参数如表7所示。

表7　优化后沉积工艺

Table 7　Optimized post-deposition process

Material	TG1/TG2-Si		TG3-Ta		ICP×2			Drum rotation/(r·min^{-1})
	Power/kW	Ar/sccm	Ar/sccm	O_2/sccm	Power/kW	Ar/sccm	O_2/sccm	
SiO_2	6	210	210	0	1	100	200	60
Ta_2O_5	6	210	210	300	/	/	/	60

采用表7工艺，制备Ta_2O_5和SiO_2薄膜，如图11所示，重新拟合光学常数，将折射率色散分布带入原膜系设计中，对反射率光谱曲线影响很小。按照原设计的膜系结构进行制备，采用台阶仪测量多层膜沉积前后样品曲率半径为122.5 m、59.1 m，并根据公式(4)计算出多层膜应力为−105 MPa。然后进行百格附着力测

试，使用百格刀和百格尺在样品表面划出百格，将3M胶带粘在样品表面，沿膜面垂直方向快速拉起胶带，重复多次，在显微镜下观察，样品未出现膜裂、脱膜等现象，如图12所示。

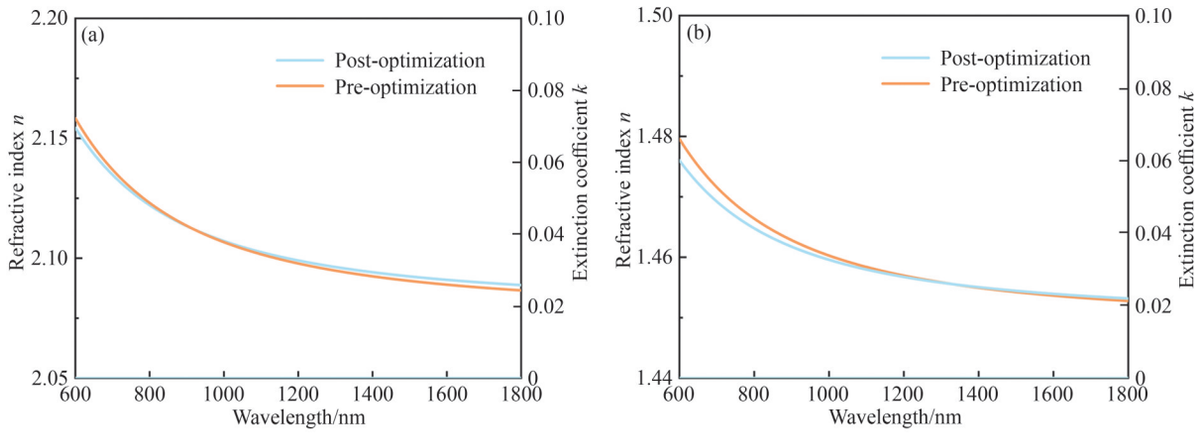


图11 Ta_2O_5和SiO_2优化前后的光学常数对比图。(a) Ta_2O_5的光学常数；(b) SiO_2的光学常数

Fig.11 Comparison of optical constants of Ta_2O_5 and SiO_2 pre- and post-Optimization. (a) Optical constants of Ta_2O_5; (b) Optical constants of SiO_2

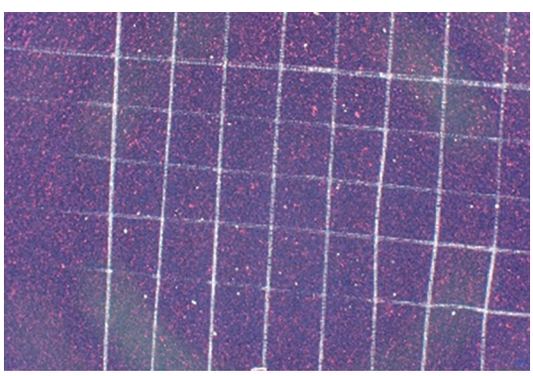


图12 百格拉膜后的表面

Fig.12 Baigla membrane diagram

3.2 光谱性能测试与分析

采用Cary7000分光光度计测量光谱，为消除基底背面反射对测量的干扰，在样品背面涂覆消光黑漆，以获取准确的反射光谱，测量结果如图13所示，在800～1 000 nm波段内的平均反射率为0.16%，在1 500～

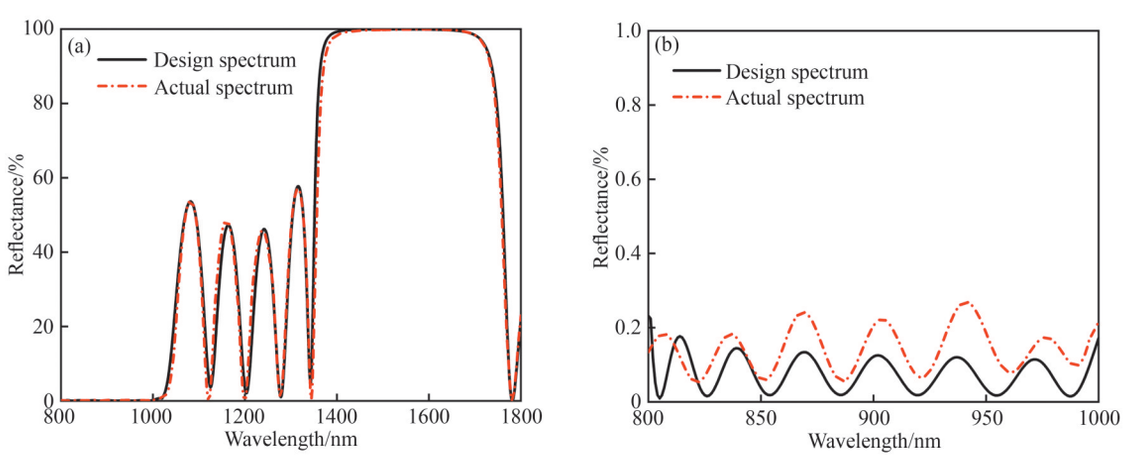


图13 分光膜理论与实测反射光谱对比图。(a)800～1 800 nm波段光谱；(b) 800～1 000 nm短波光谱

Fig.13 Comparison of theory and measured reflection spectra of the optical film. (a) 800～1 800 nm spectral range; (b) 800～1 000 nm shortwave spectrum

1 600 nm平均反射率为99.87%，满足指标要求。其中在800～1 000 nm波段实际光谱与设计光谱相比反射略微升高，如图13(b)所示，其主要原因是制备的分光膜层数多，膜层表面粗糙度会导致薄膜界面散射，引起反射率上升。

采用Zygo激光干涉仪对样品镀膜前后表面粗糙度进行表征，如图14(a)所示，镀膜前，铒玻璃基底均方根粗糙度(Rq)值为0.624 nm。如图14(b)所示，镀膜后，溅射功率会对薄膜表面造成冲击，导致孔洞的形成，增大了粗糙度[23]，测量结果显示，膜层的Rq值增至2.413 nm。

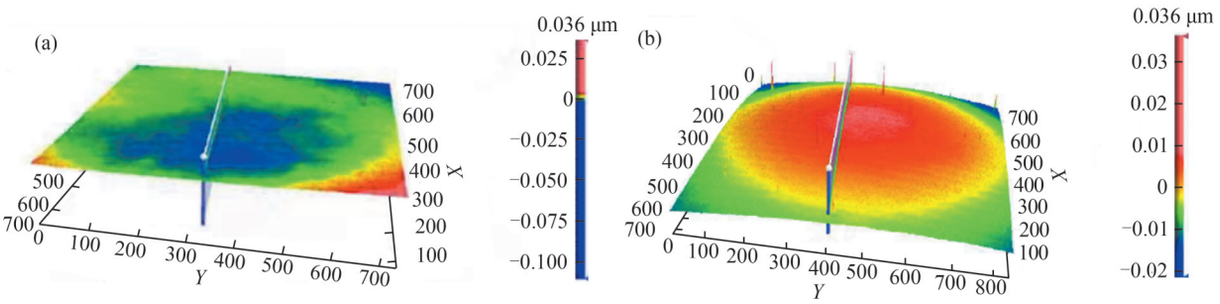


图14　样品镀膜前后粗糙度对比。(a)镀膜前；(b)镀膜后

Fig 14　Comparison of surface roughness pre- and post- thin-film deposition. (a) Pre-deposition; (b) Post-deposition

3.3　环境测试

按GJB2485A-2019光学膜层通用规范对样品进行相应的环境测试。

1) 高低温测试

将样品置于冷热交替箱内，先在(－45±5) ℃低温下保持3 h，再在(120±5) ℃高温下保持3 h，进行4个冷热循环后取出观察，样品未出现膜裂、脱膜等。

2) 水煮测试

设定温度80 ℃后，将样品放置水中，水煮6 h，样品在常温下静置2 h之后，未出现气泡，脱落等现象。

4　结论

针对激光测距系统对铒玻璃的参数要求，在铒玻璃基底上研制了近红外低应力分光膜。基于膜系设计理论，采用Ta_2O_5和SiO_2作为镀膜材料，结合沉积设备的控制工艺，利用Macleod软件进行优化设计；通过对工艺的优化，获得低应力的薄膜制备工艺；制备的薄膜样品，在800～1 000 nm波段的平均反射率为0.16%，1 500～1 600 nm波段平均反射率为99.87%，膜层残余应力为－105 MPa。所制备的样品通过了环境测试，满足激光测距系统中分光膜的使用需求。随着激光能量的增加，激光与膜层热力耦合相互作用，残余应力会增加膜层失效的风险，如何进一步降低膜层应力，是下一步研究的重点。

参考文献

[1] XU Cuilian, WANG Binke, LIU Jing. Output characteristics of Er^{3+}: Yb^{3+} co-doped phosphate glass laser[J]. Study on Optical Communications, 2013, (1): 36-38.
徐翠莲，王斌科，刘静. Er^{3+}:Yb^{3+}共掺磷酸盐玻璃激光器输出特性研究[J]. 光通信研究, 2013, (1): 36-38.

[2] GUO Junchao, HAN Yaofeng, HOU Fengqian, et al. Design of pulsed constant-current drive power supply for erbium-glass laser rangefinder[J]. Laser Journal, 2021, 42(8): 23-27.
郭俊超，韩耀锋，侯风乾，等. 铒玻璃激光测距机的脉冲恒流式驱动电源设计[J]. 激光杂志, 2021, 42(08): 23-27.

[3] ZHANG Yin, LI Mingming, LI Jun, et al. Optical properties of Er^{3+}/Yb^{3+}co-doped phosphate glass system for NIR lasers and fiber amplifiers[J]. Ceramics International, 2018, 44(18): 22467-22472.

[4] EDOUART D, GIBERT F, CENAC C. 1.645 μm Er:YAG single-mode dual-wavelength emitter for CH_4 differential absorption lidar[J]. Optics Letters, 2024, 49(21): 5997-6000.

[5] CHEN Jinyu, WANG Jin, WEI Wei, et al. Efficacy analysis of tazarotene combined with 1 550 nm erbium-glass fractional laser in repairing facial atrophic acne scars[J]. Chinese Journal of Aesthetic Medicine, 2023, 32(3): 87-91.
陈晋宇，王进，卫伟，等. 他扎罗汀联合1 550 nm铒玻璃点阵激光修复面部凹陷性痤疮瘢痕效果分析[J]. 中国美容医学, 2023, 32(3): 87-91.

[6] SONG Xinxiang, ZHANG Xiaoxia, DONG Meifeng, et al. Er^{3+}: Yb^{3+} co-doped phosphate laser glass and its applications

[J]. Laser & Optoelectronics Progress, 2004, 41(9): 33.
宋新祥,张晓霞,董梅峰,等.共掺Er^{3+}:Yb^{3+}的磷酸盐激光玻璃及其应用[J].激光与光电子学进展, 2004, 41(9): 33.
[7] YAN Jingping, DENG Lu, HU Lili. Research progress on structure and properties of phosphate glasses[J]. Journal of the Chinese Ceramic Society, 2022, 50(4): 1006-1021.
严静萍,邓路,胡丽丽.磷酸盐玻璃结构与性能的研究进展[J].硅酸盐学报, 2022, 50(4): 1006-1021.
[8] YUAN Wenjia, SHEN Weidong, ZHENG Xiaowen, et al. Optical, mechanical properties and microstructure of Nb_2O_5、Ta_2O_5 and SiO_2 thin films prepared by ion beam sputtering[J]. Acta Optica Sinica, 2017, 37(12): 364-371.
袁文佳,沈伟东,郑晓雯,等.离子束溅射制备Nb_2O_5、Ta_2O_5和SiO_2薄膜的光学、力学特性和微结构[J].光学学报, 2017, 37(12): 364-371.
[9] LIU Baojian, DUAN Weibo, LI Daqi, et al. Effects of annealing temperature on structure and stress characteristics of Ta_2O_5/SiO_2 multilayer reflective coatings[J]. Acta Physica Sinica, 2019, 68(11): 172-178.
刘保剑,段微波,李大琪,等.退火温度对Ta_2O_5/SiO_2多层反射膜结构和应力特性的影响[J].物理学报, 2019, 68(11): 172-178.
[10] ELO R, JACOBSON S, KUBART T. Tailoring residual stresses in CrN_x films on alumina and silicon deposited by high-power impulse magnetron sputtering[J]. Surface and Coatings Technology, 2020, 397: 125990.
[11] ZHU Jingtao, GUO Sheng, ZHAO Jiaoling, et al. Microstructure and stress of Zr thin films deposited by pulsed DC sputtering[J]. Acta Optica Sinica, 2021, 41(18): 255-260.
朱京涛,郭胜,赵娇玲,等.脉冲直流溅射Zr薄膜的微结构和应力研究[J].光学学报, 2021, 41(18): 255-260.
[12] BARTSCHI M, SCHACHTLER D, SCHWYN-THÖNY S, et al. Investigation of the influence of plasma source power on the properties of magnetron sputtered Ta_2O_5 thin films[C]. EPJ Web of Conferences. EDP Sciences, 2021, 255: 03005.
[13] ZHOU Y, LIU Y, SONG H, et al. Improving the adhesion of diamond-like carbon films on glass substrate by chemical etching and oxygen plasma treatment[J]. Vacuum, 2023, 218: 112629.
[14] WANG Tong, XU Junqi, LI Yang, et al. Design and fabrication of anti-reflection laser coatings on chalcogenide glass substrates[J]. Surface Technology, 2024, 53(12): 252-259.
王通,徐均琪,李阳,等.硫系玻璃基底减反射激光薄膜的设计及制备[J].表面技术, 2024, 53(12): 252-259.
[15] TIAN Xiaoxi. A Study on the Thermodynamic matching between substrate and thin films in optical coating technology [D]. Beijing: University of Chinese Academy of Sciences (Institute of Optics and Electronics, Chinese Academy of Sciences), 2020.
田晓习.光学薄膜技术中的基片与薄膜热力学匹配问题研究[D].北京:中国科学院大学(中国科学院光电技术研究所), 2020.
[16] WEN Jiahui, ZHU Meiping, SUN Jian, et al. Research progress in absorption loss control of laser coatings[J]. Acta Optica Sinica, 2022, 42(7): 9-22
温家慧,朱美萍,孙建,等.激光薄膜吸收损耗控制研究进展[J].光学学报, 2022, 42(07): 9-22.
[17] WANG B, ZHANG J, LIU H, et al. Effect of ion-assisted deposition energy of RF source on optical properties, microstructure, and residual stress of HfO_2 thin films[J]. Coatings,2024, 14(12): 1616.
[18] LI Yang, XU Junqi, LIU Zheng, et al. Influence of residual stress on surface morphology of dielectric high-reflectance coatings[J]. Chinese Journal of Vacuum Science and Technology, 2021, 41(5): 484-490.
李阳,徐均琪,刘政,等.残余应力对介质高反膜面型影响的研究[J].真空科学与技术学报, 2021, 41(05): 484-490.
[19] WANG Shengzhao, ZHANG Dan. Progress in thin film stress measurement methods [J]. Journal of Nanyang Institute of Technology, 2012, 4(4): 67-72.
王生钊,张丹.薄膜应力测量方法进展[J].南阳理工学院学报, 2012, 4(4): 67-72.
[20] LIU Y M, HAN R Q, LIU F, et al. Sputtering gas pressure and target power dependence on the microstructure and properties of DC-magnetron sputtered AlB2-type WB2 films[J]. Journal of Alloys and Compounds, 2017, 703: 188-197.
[21] LIU Feng, MENG Yuedong, REN Zhaoxing, et al. Microstructure and mechanical properties of CrN films deposited by inductively coupled plasma enhanced radio frequency magnetron sputtering[J]. Plasma Science and Technology, 2008, 10(3): 340.
[22] ZHANG Hanyan, ZHENG Danxu, SHEN Yi, et al. Insulation properties of silicon oxide (SiOx) films prepared by mid-frequency magnetron reactive sputtering[J]. Vacuum, 2023, 60(2): 34-38.
张汉焱,郑丹旭,沈奕,等.中频磁控反应溅射氧化硅(SiOx)薄膜绝缘性的研究[J].真空, 2023, 60(2): 34-38.
[23] WU Yuling. Study on the preparation and properties of HfO_2/SiO_2 optical thin films by magnetron sputtering [D]. Chengdu: University of Electronic Science and Technology of China, 2024.
吴钰铃.磁控溅射制备HfO_2/SiO_2光学薄膜及性能研究[D].成都:电子科技大学,2024.

Low-stress Near-infrared dichroic Beam-splitting Coatings on Erbium Glass Substrates for Laser Ranging Systems

ZHANG Jing[1], WANG Chong[1,2], WANG Yang[3], JIN Haijun[3], Zeng Bin[4], PAN Yonggang[1,2], YANG Fei[5], HUANG Yazhou[1,2]

(1 *College of Optoelectronic Engineering, Changchun University of Science and Technology, Changchun* 130022, *China*)

(2 *Zhongshan Research Institute, Changchun University of Science and Technology, Zhongshan* 528436, *China*)

(3 *Guangchi Technology (Shanghai) Co., Ltd., Shanghai* 200444, *China*)

(4 *Hansen Optoelectronic Materials Co., Ltd., Chengdu* 611934, *China*)

(5 *Changchun Institute of Optics, Fine Mechanics and Physics, Chinese Academy of Sciences, Changchun* 130033, *China*)

Abstract: Erbium glass lasers offer advantages such as compact size, high efficiency, and excellent beam quality. Additionally, the 1 535 nm wavelength falls within the atmospheric transmission window, exhibits strong penetration capability, and lies in the eye-safe range, significantly reducing operational risks. These lasers are widely used in laser ranging systems and also hold important applications in fields such as lidar and military medicine. However, the weak stability, hydrophilicity, and high thermal expansion coefficient of erbium glass often lead to excessive stress in thin-film devices, resulting in poor adhesion—a critical technical bottleneck limiting the development of erbium glass lasers. Research on reducing residual stress and improving thin-film adhesion on erbium glass substrates remains scarce. To address this, this study employs the control variable method combined with magnetron sputtering technology to optimize three key process parameters—argon (Ar) flow rate, target (TG) power, and inductively coupled plasma (ICP) power—thereby reducing thin-film stress and enhancing the adhesion of erbium glass thin-film devices.

First, the optical constants of the erbium glass substrate were determined using a Cary7000 spectrophotometer. Based on optical thin-film design theory, Ta_2O_5 and SiO_2 were selected as coating materials for the near-infrared band. The initial film structure was designed as Sub |$(0.5LH0.5L)^S$| Air, with the reflection bandwidth formula confirming a bandwidth of 355.2 nm at the central wavelength of 1 535 nm, meeting the specifications. The reflectivity formula indicates that, for a given ratio of high-to-low refractive indices, reflectivity increases with the number of film periods (S). To achieve a reflectivity of 99.9%, at least 12 periods were required, resulting in the finalized structure: Sub|$(0.5LH0.5L)^{12}$|Air. The film design was globally optimized using Macleod software, yielding the following configuration: Sub| 1.06H 0.76L 0.97H 0.86L 1.16H 1.11L 0.93H 0.92L H 1.08L H 0.93L 0.96H 1.06L 1.03H 0.94L 0.93H 1.02L 1.08H 1.02L 0.87H 0.96L 0.75H 0.49L |Air. Theoretical spectra showed an average reflectivity of 0.076% in the 800~1 000 nm band and 99.92% in the 1 500~1 600 nm band. Based on the robustness principle and considering deposition process constraints, manufacturability was improved by introducing film thickness error analysis. Subsequently, a beam-splitting film sample was prepared following standard deposition processes.

After deposition, adhesion testing was performed using 3M tape pressed onto the film surface and rapidly peeled off vertically five times, revealing delamination. Comprehensive analysis indicated that film delamination was primarily caused by thin-film stress, which consists of intrinsic stress and thermal stress. To address this issue, the study focused on optimizing deposition parameters and temperature variations during coating. By analyzing the influence of deposition parameters on single-layer film stress using the Stoney formula and thermal stress equations, the following trends were observed: The stress of Ta_2O_5 and SiO_2 single-layer films decreased with increasing Ar flow rate. The stress of Ta_2O_5 and SiO_2 single-layer films initially decreased and then gradually increased with rising TG power. The stress of Ta_2O_5 and SiO_2 single-layer films increased with higher ICP power. A low-stress film preparation process was identified, and the curvature radii of the samples were measured before and after deposition using an ET-4000A step profiler. The calculated multilayer film stress was -105 MPa, and subsequent adhesion tests showed no delamination.

The final beam-splitting film prepared on the erbium glass substrate exhibited an average reflectivity of 0.16% in the 800~1 000 nm band and 99.87% in the 15 00~1 600 nm band, meeting the specifications. The slightly higher reflectivity in the 800~1 000 nm band compared to the design spectrum was attributed to surface roughness-induced interfacial scattering in the multilayer film. This was further analyzed using a Zygo laser interferometer to measure surface roughness. After undergoing environmental tests in

accordance with specifications, the film showed no defects such as cracking, delamination, or bubbles. As laser energy increases, the thermo-mechanical coupling interaction between the laser and the film raises the risk of film failure due to residual stress. Further reducing film stress remains a key focus for future research.

Key words: Erbium glass; Near-infrared dichroic beamsplitter coating; Mid-frequency magnetron sputtering; Process optimization; Low stress

OCIS Codes: 310.4165; 310.4925; 310.6860

CSTR: 32255.14.gzxb20265501.0131004

Foundation item: Zhongshan Innovative Research Team Program (CXTD2023008), Jilin Provincial Science & Technology Development Program (20230101008JC), Outstanding Member of CAS Youth Innovation Promotion Association (Y202053), National Natural Science Foundation of China (11973040)